Article:
Kobayashi, Takeshi, Reid, Joshua Elias Samuel James, Shimizu, Seishi et al. (2017) The properties of residual water molecules in ionic liquids: a comparison between direct and inverse Kirkwood-Buff approaches. Physical Chemistry Chemical Physics. pp. 18924-18937. ISSN: 1463-9084

https://doi.org/10.1039/c7cp03717a

Journal Name

ARTICLE TYPE

Cite this: DOI: 10.1039/xxxxxxxxxx

The properties of residual water molecules in ionic liquids: a comparison between direct and inverse Kirkwood-Buff approaches

Takeshi Kobayashi,[a] Joshua E. S. J. Reid,[b,c] Seishi Shimizu,[b] Maria Fyta,[a] and Jens Smiatek[a,*]

Received Date
Accepted Date

DOI: 10.1039/xxxxxxxxxx

www.rsc.org/journalname

We study the properties of residual water molecules at different mole fractions in dialkylimidazolium based ionic liquids (ILs), namely 1-ethyl-3-methylimidazolium tetrafluoroborate (EMIM/BF4) and 1-butyl-3-methylimidazolium tetrafluoroborate (BMIM/BF4) by means of atomistic molecular dynamics (MD) simulations. The corresponding Kirkwood-Buff (KB) integrals for the water-ion and ion-ion correlation behavior are calculated by a direct evaluation of the radial distribution functions. The outcomes are compared to the corresponding KB integrals derived by an inverse approach based on experimental data. Our results reveal a quantitative agreement between both approaches, which paves a way towards a more reliable comparison between simulation and experimental results. The simulation outcomes further highlight that water even at intermediate mole fractions has a negligible influence on the ion distribution in the solution. More detailed analysis on the local/bulk partition coefficients and the partial structure factors reveal that water molecules at low mole fractions mainly remain in the monomeric state. A non-linear increase of higher order water clusters can be found at larger water concentrations. For both ILs, a more pronounced water coordination around the cations when compared to the anions can be observed, which points out that the IL cations are mainly responsible for water pairing mechanisms. Our simulations thus provide detailed insights in the properties of dialkylimidazolium based ILs and their effects on water binding.

1 Introduction

Room-temperature ionic liquids (ILs) are versatile solvents for many technological applications and chemical synthesis protocols. As few examples, ILs can be used as media for chemical or catalytic reactions[1–3], as electrolytes in electrochemical devices[4–6] or as solvents for various polar and apolar solutes[7]. In contrast to beneficial properties like low flammability, low volatility and low melting points, the use of ILs for practical purposes is often limited by their high hygroscopicity. Thus, even low amounts of water in the IL crucially influence the performance and modify thermophysical properties in addition to the structural organization of the solution when compared to pure ILs[8–21]. As a prominent example, the influence of water significantly diminishes the broad electrochemical window known for pure ILs, such that the practical usability of ILs in electrochemical devices is still under debate[19].

In order to understand the profound hygroscopicity of ILs, several experiments and simulations were performed[9,13,17,22–27]. An extensive discussion of the resulting effects can be found in recent reviews[16,28]. The outcomes of most studies revealed that low water concentrations induce the formation of residual water states in the IL[9,18]. Further studies highlighted that water molecules accumulate around the hydrophobic parts of the ions with a strong affinity towards the anions[29,30]. In agreement with previous results, it was reported that hydrophilic ILs show a tendency of pronounced water-anion network formation[31,32] and that even hydrophobic ILs attract high amounts of water[8,33]. The pronounced hygroscopicity of hydrophobic ILs was explained by the occurrence of water clusters at low and intermediate water mole fractions[20,21]. Although hygroscopic properties are typical for all IL classes, ranging from protic to aprotic ILs, a recent publication highlighted slight differences[21]. Thus, the strength of ion-water interactions changes for different ILs with varying water content whereas ion-ion interactions are only weakly affected by the presence of water[21]. As a conclusion, the formation of water clusters

[a] Institute for Computational Physics, University of Stuttgart, Allmandring 3, 70569 Stuttgart, Germany
[b] York Structural Biology Laboratory, Department of Chemistry, University of York, Heslington, York YO10 5DD, United Kingdom
[c] TWI Ltd., Granta Park, Great Abington, Cambridge CB21 6AL, United Kingdom
* smiatek@icp.uni-stuttgart.de

was often inferred for intermediate concentrations in apolar and thus hydrophobic ILs[20,21].

For low content of water, it was shown that even homologues of common IL cations, *i. e.* dialkylimidazolium, show a distinct water affinity[20,24,30]. This finding becomes even more important in terms of computer simulations, which showed the formation of apolar and polar regions in neat dialkylimidazolium ILs with long alkyl chains[34]. Other simulation results revealed the perturbation of the apolar domains by water molecules for the full range of water mole fractions[13], which was confirmed by experiments, such that the diffusivity and ionic conductivity[35–37], as well as the viscosity of the IL solution changes when compared to pure ILs[38]. Additional outcomes of simulations also indicated the change of interactions between IL species and solvent molecules for low mole fractions of ILs[39]. In agreement with numerical findings, recent experimental results also highlighted an order of magnitude larger diffusivity of water molecules in comparison to the IL ions[40,41].

As it was discussed above, the presence of water molecules thus seriously harms the overall performance of the solution, which is most important for ILs in electrochemical devices. In more detail, water molecules tend to accumulate in the electric double layer around the electrodes[19]. As a result, the local number of water molecules around the electrodes increases at higher apparent voltages, such that the width of the electrochemical window becomes smaller when compared to neat ILs[19].

Whereas most of the above-mentioned investigations focused on low water concentrations, recent reviews and studies also discussed the opposite case in terms of low concentrated ionic liquids in aqueous solution[16,39,42–53]. It was pointed out, that these so-called aqueous ILs have a broad applicability in several biotechnological processes and protein stabilization mechanisms[43,46,47]. Moreover, it was argued that ion-specific effects in combination with kosmotropic and chaotropic properties, accounting also for the local interaction with the water shell,[16,43,46,47] crucially influence the solution behavior. Although it was shown that ion-ion interactions are not weakened in presence of residual water molecules[21], it can be assumed that the presence of water has some impact on the general IL solvation behavior. For instance, a complex interplay between anion and cation solvation mechanisms was reported[34,44,54–64], implying that the presence of water seriously affects the corresponding solvation behavior. Although this is an important point, these effects have sparingly been investigated.

In order to study the water properties in ILs for intermediate and low water mole fractions, we performed atomistic molecular dynamics (MD) simulations of water molecules at different concentration in 1-ethyl-3-methylimidazolium tetrafluoroborate and 1-butyl-3-methylimidazolium tetrafluoroborate, respectively, which are in the following abbreviated by EMIM/BF4 and BMIM/BF4. The study of these ILs was motivated by previous findings in terms of alkyl chain length effects[24,34] and controversial results for low water mole fractions as it was discussed above. For the first time, in order to provide a consistent view on the molecular structure, we compare Kirkwood-Buff integrals directly computed through simulations with Kirkwood-Buff integrals computed from experimental results through an inverse approach. The good agreement between both approaches verifies our simulation model. All corresponding results reveal a complex interplay between water-water, water-ion and ion-ion accumulation effects. Through our simulations, we are able to rationalize the experimental findings with regard to a consistent molecular interpretation. In this respect, our study highlights the combined benefits of direct and inverse Kirkwood-Buff theory as a useful tool to verify simulations and to achieve deeper insights into the properties of molecular structures when these are not easily accessible through experiments.

The remainder of the article is organized as follows: a brief introduction into the direct and the inverse Kirkwood-Buff theory is presented in the next section, followed by a discussion of the simulation details. The results will be presented in section 4. We will summarize and conclude in the last section.

2 Theoretical Background

2.1 Kirkwood-Buff theory

A consistent description for IL-water mixtures, based on thermodynamic and statistical mechanics arguments is provided by the Kirkwood-Buff (KB) theory, which was originally developed as a molecular theory of solutions and solution mixtures[47,65–81]. It has to be noted that the KB theory does not imply any restrictions on the molecular structure of the water molecules and the ion species, such that the theory is applicable for all systems in the liquid state. For different ion species, the introduction of an indistinguishable ion approach is necessary[70,82]. Hence, cations and anions have to be considered as one single species, which we denote in the following as *ions*. In this context, simulations allow us to study the binding of species to individual ions in more detail and to obtain results which are inaccessible to inverse KB approaches, as we will point out in the remainder of this article.

In our study, we focus on the analysis of the binding behavior between the ions, as denoted by the index '2' and water molecules with the index '1'. In this way, three local binding modes according to ion-ion, water-water and ion-water binding can be defined. For the analysis, the KB integral, which is the most essential ingredient of the KB theory is defined as

$$G_{ij} = 4\pi \int_0^\infty r^2 [g_{ij}(r) - 1] \, \mathrm{d}r \tag{1}$$

which can be approximated by

$$G_{ij} \approx G_{ij}(r_c) = 4\pi \int_0^{r_c} r^2 [g_{ij}(r) - 1] \, \mathrm{d}r \tag{2}$$

where $g_{ij}(r)$ corresponds to the radial distribution function between two species i and j, and r_c is a finite cutoff distance as defined through $g_{ij}(r) = 1$ for all values $r \geq r_c$[68,71,81]. The KB integrals can be interpreted as excess volumes corresponding to the non-ideal distribution of molecular species with the requirement of symmetry, $G_{ij} = G_{ji}$. In contrast to an ideal gas, real molecules of species k have a fixed size a_k, such that all values $G_{ij}(a_k) < 0$ for $r \leq a_k < r_c$ expressing the excluded volume of the molecule. Moreover, one can find $G_{ij}(a_k) < G_{ij}(a_n)$ for $a_k > a_n$. The corresponding number of excess particles or molecules can

be calculated by $N_{ij}^{xs} = \rho_j G_{ij}$ with the bulk number density ρ_j and the additional requirement $N_{ij}^{xs} \neq N_{ji}^{xs}$. Although the original KB theory and the KB integrals were formulated in order to describe molecular fluctuations in the grandcanonical μVT ensemble, it was shown that identical expressions can be derived equivalently in several other ensembles and specifically in the NVT and the NpT ensemble[69,83]. We point the reader to Refs. 66,67,69,73,81 for a more detailed overview on the KB theory.

More detailed approaches to study charged systems in terms of the KB theory can be found in Refs. 82,84–87 and for ILs in Refs. 20,21. Hence, assuming that IL cations and anions contribute equivalently, one can define the ion-ion KB integral G_{22} in presence of cations $(+)$ and anions $(-)$ according to[88–90]

$$G_{22} = \left(\frac{n_+}{n_\pm}\right)^2 G_{++} + \left(\frac{n_-}{n_\pm}\right)^2 G_{--} + \frac{n_+ n_-}{n_\pm^2}(G_{+-} + G_{-+}) \quad (3)$$

with $n_\pm = n_+ + n_-$ and $G_{+-} = G_{-+}$, where n_j with $j = +,-$ denotes the number of ion species or stoichiometric coefficients in the corresponding ion dissociation/association equilibrium. The resulting KB integral for ion-solvent interactions is defined by

$$G_{21} = G_{12} = \frac{n_+}{n_\pm} G_{+1} + \frac{n_-}{n_\pm} G_{-1} \quad (4)$$

with $G_{21} = G_{\pm 1} = G_{1\pm}$.

Based on the KB integrals, one can define a preferential binding coefficient[73,81]

$$\nu_{ji} = \rho_i (G_{ji} - G_{jj}) \quad (5)$$

with $i, j = 1, 2$ and $i \neq j$. For values $\nu_{ji} > 0$, one can observe a preferential binding of species i to species j according to the relation[73,81]

$$\nu_{ji} = N_{ji}^{xs} - \frac{\rho_i}{\rho_j} N_{jj}^{xs} \quad (6)$$

and equivalently, a preferential exclusion for $\nu_{ji} < 0$[47]. The preferential binding coefficient at a temperature T with the Boltzmann constant k_B is also connected with the transfer free energy[47]

$$F_{ji}^* = -k_B T \nu_{ji} \quad (7)$$

which estimates the free energy that is needed to bring two species infinitely apart in close contact.

Although the KB integrals and the KB theory can be derived from rigorous statistical mechanical arguments, some problems in their computational evaluation remain unresolved. The KB integrals need to show a good convergence at large distances in order to provide reasonable values. Recently, several techniques were proposed in order to achieve this aim and to introduce further modifications in computer simulations[91–95]. An older approach also corrects the values of KB integrals in closed systems[96]. Accordingly, it is possible to deduce reliable results even from non-convergent KB integrals. Specifically, for long-range ordered fluids like ILs[44], the evaluation of these values is a challenging task. Fortunately, if the underlying radial distribution function $g_{ij}(r)$ is well-behaved at large distances, *i. e.* showing regulatory oscillations with approximately constant periods, the values of $G_{ij}(r)$ for $r \gg 1$ nm oscillate around a constant number as well. In this respect, the running average $\bar{G}_{ij}(r)$ in this region fluctuates around G_{ij} and establishes the relation $\bar{G}_{ij}(r) \approx G_{ij}$. The fluctuations can be used to determine the standard deviation of G_{ij}.

Another problem arises due to the constraints of the indistinguishable ion approach, which prohibits a more detailed analysis of the water binding behavior to the individual ion species. The limitations of the KB integrals for standard simulation approaches[91–93] can be circumvented by introducing the local/bulk partition coefficient[72,97,98],

$$K_{ij}^p = \frac{\langle N_{pi}(r)\rangle / \langle N_{pj}(r)\rangle}{N_i / N_j} \quad (8)$$

with $i, j, p = 1, 2, +, -$, and the definition $\langle \cdots \rangle$ for the average local number of molecules of species i in comparison to species j around molecules of species p. The total number of molecules is defined by the relation $N_i = \rho_i \cdot V$ with volume V and the cumulative local number of molecules

$$N_{ij}(r) = 4\pi\rho_j \int_0^r r^2 g_{ij}(r) \mathrm{d}r \quad (9)$$

can be used to calculate coordination numbers $N_{ij}(d)$ around specific molecules by integration of Eqn. (9) up to a specific distance d, usually including the first solvation shell.

Although a direct connection between the local/bulk partition coefficient and the KB theory is questionable[98], a preferential exclusion or a preferential binding mechanism of species indeed can be detected[44,99–101]. For instance, at short distances in the local region around the reference molecule, values of $K_p > 1$ and $K_p < 1$ indicate a preferential binding or a preferential exclusion behavior, respectively. Hence, it is possible to compute different local/bulk partition coefficients in order to distinguish between cation and anion properties. Accordingly, the local/bulk partition coefficient provides a simple and reliable analysis tool for binding properties in computer simulations[44,47].

2.2 Inverse Kirkwood-Buff theory

Whereas the direct KB approach relies on an evaluation of the known radial distribution function, the inverse KB theory focuses on thermodynamic and experimental data for the calculation of the KB integrals in several mixtures[69,102] and thus also in water-IL solutions[20,21]. In the following, we briefly sketch the derivation of KB integrals for binary solutions and more specifically for IL-water mixtures. More detailed informations can be found in Refs. 20,21.

Using the well-known relation for the derivative of the water chemical activity[20,81]

$$a_{11} = \left(\frac{\partial \mu_1}{\partial \ln \rho_1}\right)_{T,p} = \left(\frac{\partial \ln a_1}{\partial \ln \rho_1}\right)_{T,p} = \frac{1}{1 + \rho_1 (G_{11} - G_{12})} \quad (10)$$

with μ_1 the chemical potential and a_1 the activity of water, one can define a chemical equilibrium according to $\mu_1^V = \mu_1$. This would be the chemical potential of the water vapor phase,

$$\mu_1^V = \mu_1^{\mathrm{int}} + k_B T \ln \rho_1^V \Lambda_1^3 \quad (11)$$

with the water vapor phase density ρ_1^V. Most importantly, the intramolecular contributions μ_1^{int} and the momentum partition function Λ_1^3 do not depend on the water liquid phase bulk number

density and thus Eqn. (10) can be rewritten according to

$$\rho_1(G_{11}-G_{12}) = \left(\frac{\partial \ln \rho_1}{\partial \ln \rho_1^V}\right)_{T,p} - 1 \tag{12}$$

as it was outlined in Ref. 20. An equivalent expression for the water-ion KB integral in agreement with Eqn. (1) can be derived from the relation

$$(\rho_1 G_{11}+1)V_1 + \rho_2 G_{12} V_2 - RT\kappa_T = 0 \tag{13}$$

where V_1, V_2 denote partial molar volumes of the species and κ_T the isothermal compressibility with the molar gas constant R. From the relation above, the corresponding KB integrals can be written as

$$G_{12} = -V_1\left(\frac{\partial \ln \rho_1}{\partial \ln \rho_1^V}\right) + k_B T \kappa_T \tag{14}$$

for the ion-water,

$$G_{11} = \frac{1}{n_1}\left(n_2 V_2 \frac{\partial \ln \rho_1}{\partial \ln \rho_1^V} - 1\right) \tag{15}$$

for the water-water KB integral and

$$G_{22} = -V_1\left(1-\frac{1}{\rho_2 V_2}\right)\left(\frac{\partial \ln \rho_1}{\partial \ln \rho_1^V}\right) - \frac{1}{\rho_2} + k_B T \kappa_T \tag{16}$$

for the ion-ion KB integral, respectively. For the evaluation of the KB integrals in the inverse KB approach, one needs experimental values for the water and ion bulk number densities in the liquid mixtures, values for the water vapor densities at specific mole fractions and the corresponding values for the partial molar volumes of water and ions in combination with the isothermal compressibility of the solution.

As an alternative, a much more compact formulation of the KB integrals can be derived by introducing the derivative of the water chemical potential with respect to the water mole fraction $x_1 \equiv x_{\mathrm{H_2O}}$, which reads

$$D = \frac{x_1}{k_B T}\left(\frac{\partial \mu_1}{\partial x_1}\right)_{T,p} = \left(\frac{\partial \ln a_1}{\partial \ln x_1}\right)_{T,p} \tag{17}$$

as it was outlined in detail in Ref. 21. Due to the fact, that our data for the inverse KB integrals rely on the original formulation, we follow the outlined approach formulated in Ref. 20. By doing so, a crucial point is the numerical evaluation of $(\partial \ln \rho_1 / \partial \ln \rho_1^V)$ in addition to the extraction of the corresponding values. A meaningful approach in order to establish a useful protocol was recently presented in Refs. 20,21.

2.3 Mean square displacement of molecules and partial structure factors

In order to study the dynamic behavior of the considered species in solution, one can calculate the mean-square displacement (MSD) of the center of mass for the corresponding molecules according to $\langle \Delta r^2(t)\rangle = \langle (\vec{R}_{cm}(t) - \vec{R}_{cm}(t_0))^2\rangle$, which is related to the Einstein expression

$$\langle \Delta r^2(t)\rangle = 6 D_{cm} \lim_{t\to\infty} t \tag{18}$$

with the diffusion coefficient D_{cm} and the center-of-mass positions $\vec{R}_{cm}$ at long times $t \to \infty$. The introduction of the parameter α according to [103]

$$\sqrt{\langle \Delta r^2(t)\rangle} \sim t^{\alpha} \tag{19}$$

allows us to distinguish between different diffusion regimes. Diffusive behavior, as indicated by $\alpha = 0.5$, dominates for long times according to the Einstein expression, and a different value of $\alpha \neq 0.5$ can be observed at shorter times or for glass-like liquids [103].

The global properties of the solution can be studied through the partial structure factors at different length scales. In particular, the use of partial structure factors was already established for IL/water mixtures [13] according to the expression

$$S_{ij}(q) = 1 + \frac{4\pi\rho_j}{q}\int_0^{\infty} r \sin(qr)[g_{ij}(r)-1]\,\mathrm{d}r \tag{20}$$

with $q = 2\pi/r$. This is equivalent to

$$S_{ij}(\vec{q}) = 1 + \rho_j \hat{G}_{ij}(\vec{q}) \tag{21}$$

with the corresponding Fourier-transformed KB integrals

$$\hat{G}_{ij}(\vec{q}) = \int_V [g_{ij}(\vec{r})-1]\, e^{-i\vec{q}\vec{r}}\,\mathrm{d}\vec{r}, \tag{22}$$

which can be further modified in terms of Fourier-transformed excess numbers of particles with $\hat{N}^{\mathrm{xs}}(\vec{q}) = \rho_j \hat{G}_{ij}(\vec{q})$, such that Eqn. (21) then reads $S_{ij}(\vec{q}) = 1 + \hat{N}^{\mathrm{xs}}(\vec{q})$. The above introduced relations highlight the fact that the partial structure factor is closely related to the functional form of the KB integrals (Eqn. (1)) and thus also accounts for excess quantities.

3 Simulation Details

All MD simulations were performed with the GROMACS 5.1.3 package [104–106]. We used OPLS/AA force fields [107,108] for the ionic liquids 1-ethyl-3-methylimidazolium and 1-butyl-4-methylimidazolium tetrafluoroborate [109], denoted in the following as EMIM/BF4 and BMIM/BF4, respectively. Different water mole fractions $\mathrm{x_{H_2O}} = \{0.0, 0.05, 0.10, 0.15, 0.20, 0.25, 0.30\}$ were simulated with the SPC/E water model [110]. We have inserted a constant and reasonable number of ion pairs [111] $N_{\mathrm{pairs}} = 1000$ for all mole fractions into a cubic box and added the corresponding number of water molecules in order to establish the required values for $\mathrm{x_{H_2O}}$. All initial cubic simulation boxes with periodic boundary conditions and an initial box length of $d = 6.5$ nm (EMIM/BF4 with water) and $d = 7.2$ nm (BMIM/BF4 with water) were filled randomly with ions and water molecules using the software package PACKMOL [112].

In all simulations, the temperature was maintained at $T = 298$ K by an improved velocity-rescaling thermostat [113], using a coupling time constant of 0.1 ps. In the NpT simulations, the pressure was kept constant at $p = 1$ bar by the Parrinello-Rahman barostat [114] (coupling time constant 2 ps, compressibility $4.5 \cdot$

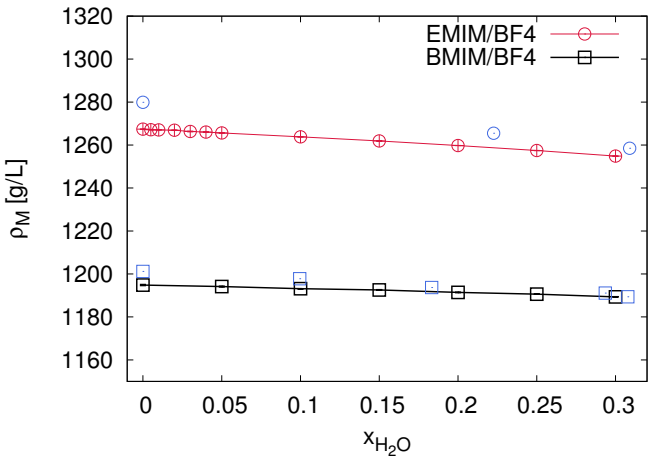

Fig. 1 Mass densities of EMIM/BF4 (simulation results: red circles with lines, experimental results[36]: blue circles) and BMIM/BF4 (simulation results: black squares with lines, experimental results[36]: blue squares) for different mole fractions of water.

10^{-5} bar^{-1}). Electrostatic interactions were treated through the Particle Mesh Ewald (PME) method[115,116], where a real-space cut-off of 1.0 nm and a grid spacing of 0.16 nm with fourth-order interpolation scheme was used. Lennard-Jones interactions were truncated at 1.0 nm and shifted to zero. The equations of motion were integrated by the Leapfrog algorithm with an elementary time step of 2 fs. All bonds involving hydrogen atoms were constrained by the LINCS algorithm[117]. An energy minimization was first performed using a steepest descend method, followed by an equilibration of the system for 10 ns under constant temperature and constant volume conditions. Subsequently, we performed another equilibration run for 10 ns under constant temperature and constant pressure (NpT). The final NpT production runs had a length of 500 ns each and snapshots were stored with a stride of 10 ps.

The experimental input values for the inverse KB approach were published in Refs. 22,27 and the values of the KB integrals were already discussed in Ref. 20. A detailed description of the protocol and further details on the calculation of the KB integrals are presented in Refs. 20,21.

4 Results

4.1 Mass densities and diffusion coefficients

In order to validate our simulation model, we first compare the obtained mass densities ρ_M with experimental data published in Ref. 36 in Fig. 1. The results for BMIM/BF4 for different mole fractions of water reveal a good agreement with the experimental data. Slight deviations can be seen for EMIM/BF4. Nevertheless, the most pronounced deviations are smaller than 2%, which highlights the validity of our simulation model in comparison to the experimental findings. Moreover, it can be seen that the addition of water to both ILs induces only a slight decrease of the mass density. Thus, for water mole fractions of $x_{H_2O} = 0.3$, a weak decrease of roughly 2% can be observed, which points to the fact that the influence of water is less important for the mass density.

A slightly different behavior can be observed for the diffusion coefficients (Fig. 2). It is known that standard atomistic force fields neglecting polarization effects quantitatively deviate from experimental findings related to the mean-square displacement of species[118,119]. However, here we are able to compare and discuss the results for the different species in a qualitative way. Accordingly, an increasing amount of water molecules significantly accelerates the diffusion of the IL cations by a factor of $4-5$ and for the anions by a factor of $7-8$. For water molecules, the diffusion becomes faster by a factor of 2 for a mole fraction of $x_{H_2O} = 0.30$ when compared to neat ILs or a mole fraction of $x_{H_2O} = 0.05$, respectively. In fact, the increased diffusivity of the ions is related to a lower viscosity of the solution as it was observed experimentally for aqueous IL mixtures[120]. It becomes evident that all species in EMIM/BF4 reveal higher diffusion coefficients when compared to BMIM/BF4. In contrast, when compared to the ions, only a weak increase in the water diffusivity can be observed. Hence, one can assume that the formation of connected water regions, resembling bulk water properties, can actually be ignored. This

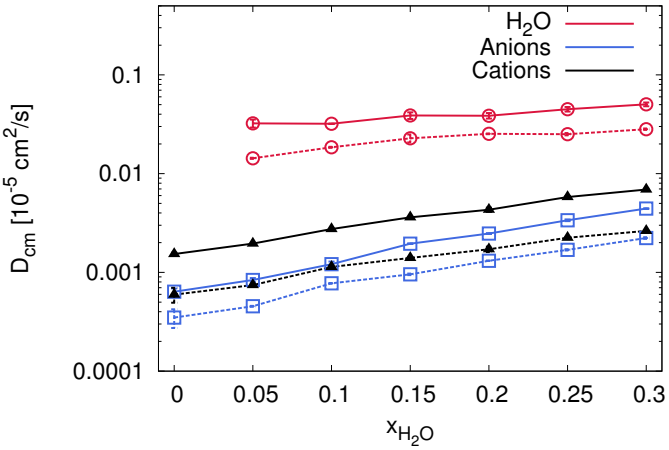

Fig. 2 Diffusion coefficients for water molecules (red circles), IL cations (black triangles) and IL anions (blue squares) for different mole fractions of water in EMIM/BF4 (symbols with solid lines) and BMIM/BF4 (symbols with dashed line).

assumption is supported by the values for the number of hydrogen bonds between water molecules. The corresponding results are shown in the supplementary material. It can be seen that the number of intermolecular water hydrogen bonds is negligibly small. With regard to the ion properties, a detailed understanding of the different increases of the anion and cation diffusivities is possible by a structural analysis of the solution, which is presented next.

4.2 Radial distribution functions: influence of water on ion-ion distributions

Due to the broad range of water mole fractions in the IL, ranging from very low with $x_{H_2O} = 0.05$ to intermediate values ($x_{H_2O} = 0.30$), one can ask if the presence of water has a significant influence on the ion distribution and if concentration-dependent effects are evident. In order to clarify these questions, we cal-

culated the radial distribution functions between the cations (+) and the anions (−) as denoted by $g_{++}(r)$ and g_{+-} for different water mole fractions. The results for EMIM/BF4 and BMIM/BF4 are presented in the top panel and the bottom panel of Fig. 3, respectively. As a first point, the quantitative agreement between

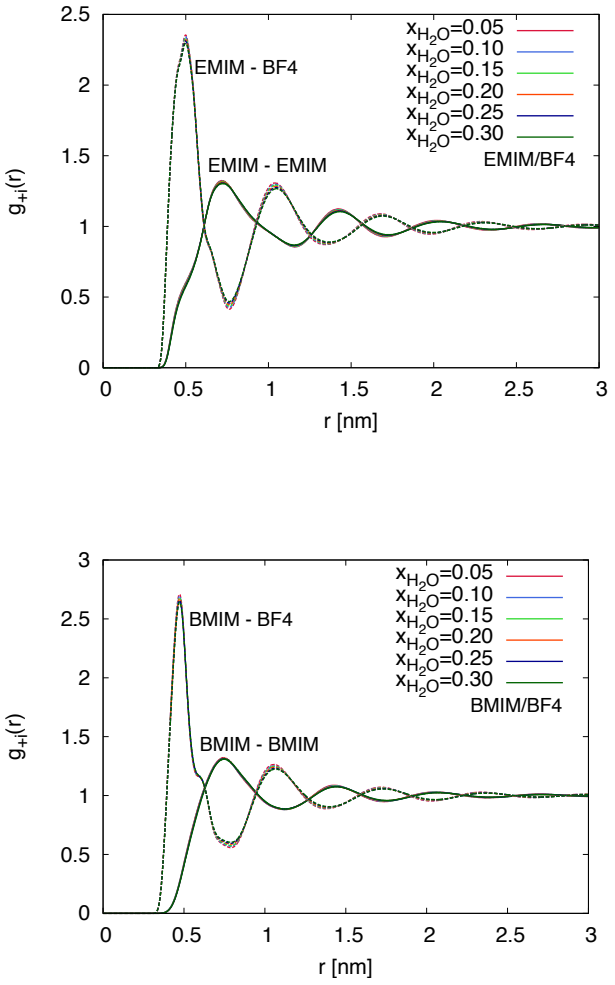

Fig. 3 Top: Radial distribution function $g_{++}(r)$ between center-of-masses for EMIM-EMIM pairs (solid lines) and $g_{+-}(r)$ for EMIM-BF4 pairs (dashed lines). Bottom: Radial distribution function $g_{++}(r)$ between center-of-masses for BMIM-BMIM pairs (solid lines) and $g_{+-}(r)$ for BMIM-BF4 pairs (dashed lines). The data are shown at different water mole fractions.

the radial distribution functions at different water content and for both ILs becomes evident. Hence, one can conclude that water, even at intermediate concentrations, has a very minor impact on the local organization of the ions. Thus, with regard to previous simulation results[13,39], where significant differences in the ion structural arrangement at higher water content were observed, it can be seen that this limiting behavior is not reached for $x_{H_2O} = 0.30$. Moreover, the individual radial distribution functions show many similarities between both ILs. Thus, the heights of the maximum values are roughly comparable and bulk solution behavior can be observed for $r \geq 2.5$ nm. In addition, it can be seen that the first peak in the cation-cation radial distribution function $g_{++}(r)$ is slightly higher than unity, which is a consequence of the strong cation-anion paring in the solution[44,121]. As a short preliminary summary, we can conclude that water has a negligible influence on the ion distribution and that the longer alkyl chain in BMIM does not significantly modify the results when compared to EMIM.

4.3 Direct and inverse Kirkwood-Buff integrals: structural properties of the solution

The radial distribution functions $g_{22}(r)$ and $g_{21}(r)$ with regard to the center-of-masses of the molecules for a water mole fraction of $x_{H_2O} = 0.30$ are depicted in Fig. 4. Inspection of $g_{21}(r)$ for both

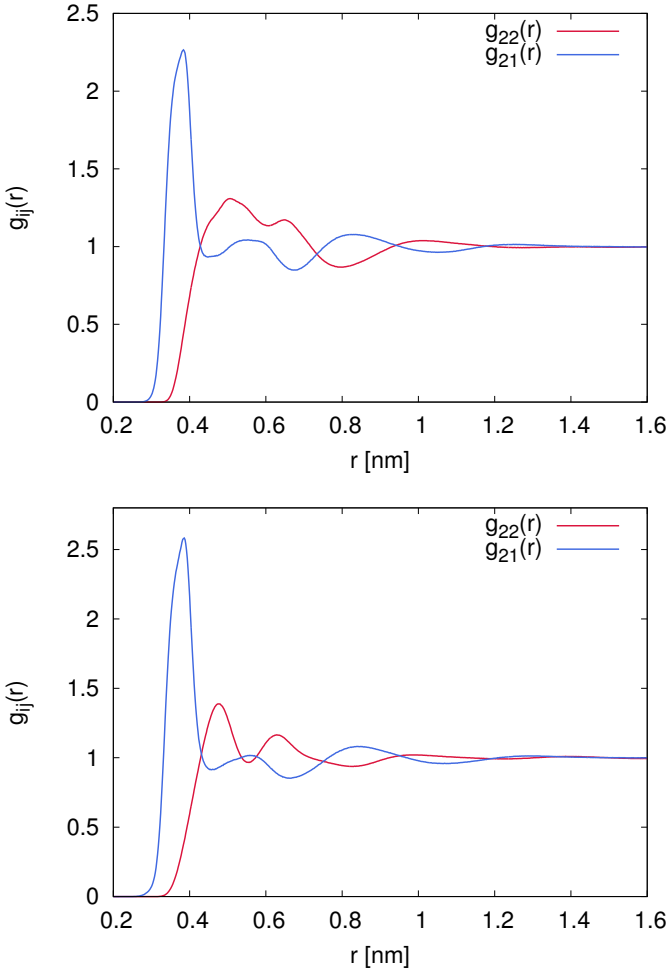

Fig. 4 Top: Radial distribution functions $g_{22}(r)$ (red line) and $g_{21}(r)$ (blue line) between center-of-masses of molecules for a water mole fraction of $x_{H_2O} = 0.30$ in EMIM/BF4. Bottom: Radial distribution functions $g_{22}(r)$ (red line) and $g_{21}(r)$ (blue line) between center-of-masses of molecules for a water mole fraction of $x_{H_2O} = 0.30$ in BMIM/BF4.

ILs clearly reveals that the first solvent shell around the ions at distances $r \leq 0.4$ nm is occupied by water molecules. Integration of the radial distribution function according to Eqn. (9) up to the distance $d = 0.4$ nm gives a coordination number of $N_{21}(d) \ll 1$, which indeed reveals that the ions are only poorly hydrated. A

well-defined second maximum can be observed at $r = 0.85$ nm, which highlights that water molecules fill the gaps between the ions. Hence, an alternating structure of ion and water shells around the reference ions can be observed, which resembles the solvation structure of differently charged model spheres in neat ILs[44,64]. Our results on $g_{22}(r)$ reveal a slightly more structured arrangement of BMIM/BF4 when compared to EMIM/BF4 due to the presence of the two maxima at $r_1 \approx 0.45$ nm and $r_2 \approx 0.65$ nm. The occurrence of these two values can be attributed to different orientations of the dialkylimidazolium cations[44]. Their absence on the contrary, results in a tighter packing, and thus a higher mass density of EMIM/BF4 when compared with BMIM/BF4 (see Fig. 1). Moreover, it has to be noticed that bulk solution behavior for water molecules around ions in both ILs ($g_{ij}(r) \approx 1$) can be observed at $r \geq 1.4$ nm.

In order to discuss the structural arrangement of the solution in the light of the Kirkwood-Buff theory, we calculated the corresponding values of G_{22}, G_{21} and $G_{21} - G_{22}$ for different mole fractions of water as described in section 2. For a more convenient comparison with the inverse KB results, we introduce the rescaled KB integrals $\tilde{G}_{ij} = N_A G_{ij}$ with the Avogadro constant N_A. The corresponding results obtained by a direct (our simulations) and an inverse (Ref. 20) KB approach are shown in Fig. 5. In general, it can be seen that an increase of water mole fractions does not significantly affect the resulting values of the corresponding KB integrals. Thus, we can conclude that concentration-dependent effects are absent. In more detail, the values for $\tilde{G}_{21}$ are slightly negative for both ILs with values around ≈ -10 cm^3/mol to ≈ -18 cm^3/mol (EMIM/BF4) and ≈ -8 cm^3/mol to ≈ -16 cm^3/mol for BMIM/BF4. In order to interpret these results, one has to discuss the meaning of $\tilde{G}_{21}$. In general, values of $\tilde{G}_{21}$ can be regarded as excess volumes with respect to water molecules around IL ions. Hence, slightly more negative values indicate a larger excluded volume as can be observed for water around EMIM/BF4 when compared to BMIM/BF4.

The arrangement of the IL species can be studied through $\tilde{G}_{22}$. The values for EMIM/BF4 and BMIM/BF4 obtained by the direct and the inverse KB approach coincide and are largely negative, lying between ≈ -78 cm^3/mol and ≈ -81 cm^3/mol (EMIM/BF4) and ≈ -95 cm^3/mol to ≈ -98 cm^3/mol for BMIM/BF4. In fact, the corresponding values linearly decrease with increasing mole fractions of water. We can conclude that the presence of water increases the excluded volume between the IL species, corresponding to a decreased mass density as it was also observed in Fig. 1. Furthermore, the excluded volume is more negative for BMIM/BF4 when compared to EMIM/BF4, which can be fully assigned to the larger molecular size of the BMIM cations. In general, the negative values for $\tilde{G}_{22}$ can be attributed to the excluded volume of the species. This evidence together with the indistinguishable ion approach points to the fact that like-charge ions strongly contribute. As a general result, our results for $\tilde{G}_{21}$ and $\tilde{G}_{22}$ reveal a good agreement between the direct and the indirect KB approach.

We next discuss the values for $\tilde{G}_{21} - \tilde{G}_{22}$. In fact, the multiplication of the original KB integrals with the water density allows us to estimate the preferential binding coefficient ν_{21} according to Eqn. (6). Inspection of the data in Fig. 5 reveals that the values for $\tilde{G}_{21} - \tilde{G}_{22}$ are strongly positive for both ILs. Larger positive values can be indeed observed for BMIM/BF4, which can be interpreted as a stronger binding of water molecules to BMIM when compared to EMIM. However, with respect to the individual values for $\tilde{G}_{21}$ and $\tilde{G}_{22}$, it can be seen that this view establishes a wrong interpretation. In fact, all values for $\tilde{G}_{21}$ and $\tilde{G}_{22}$ are negative and thus the positive values for $\tilde{G}_{21} - \tilde{G}_{22}$ imply that it is less beneficial for IL ions to accumulate around complementary ions when compared to water molecules. The larger values for BMIM/BF4 do not indicate a more favorable interaction with water molecules when compared with EMIM, but can be fully attributed to the more negative values for $\tilde{G}_{22}$ and are due to these reasons mostly influenced by size effects. Furthermore, it can again be seen that concentration-dependent effects are absent and therefore we can assume that water molecules at low mole fractions below $x_{H_2O} = 0.3$ do not form large water domains.

Snapshots of the corresponding systems for $x_{H_2O} = 0.3$ are depicted in Fig. 6. It can be clearly seen that pronounced water domains are absent and that only smaller water clusters are formed. The presence of water dimers and higher molecular clusters can be observed at some positions, but most water molecules remain in the monomeric state around the ions. This finding is in good agreement with previous assumptions[21], where only the presence of small water clusters in EMIM/BF4 and BMIM/BF4 was discussed.

4.4 Local/bulk partition coefficients: water-ion and water-water pairing

As we discussed in the last subsection, the application of both KB approaches is limited by the application of the indistinguishable ion approach. Specifically the inverse KB theory hampers from this constraint, but as we will show in the following, this drawback can be circumvented by simulations, such that the combination of both approaches provides a detailed study of the system properties in good agreement with experimental results.

In order to study the local binding behavior of water molecules to cations and anions, we calculated the radial distribution functions $g_{+1}(r)$ and $g_{-1}(r)$ at different water content for both ILs. The results are depicted in Fig. 7. In agreement with all previous results, it can be clearly seen that concentration dependent effects are absent. Thus, the corresponding values for the individual radial distribution functions at different x_{H_2O} coincide for both ILs. Moreover, it becomes evident that the maximum peak values in $g_{-1}(r)$ for water molecules around anions are significantly higher when compared with the cation-water binding in $g_{+1}(r)$. A slight difference in the maximum values can be also observed between BF4 and water molecules in BMIM/BF4 and EMIM/BF4. Hence, the maximum potential of mean force as defined by

$$\Delta F^{\pm}_{\mathrm{PMF}} = -k_B T \log\left(\frac{g_{\pm 1}(r_M)}{g_{\pm 1}(r_\infty)}\right) \tag{23}$$

with the peak value position r_M in the first coordination shell and $g_{\pm 1}(r_\infty) = 1$ is highest for anion-water binding in

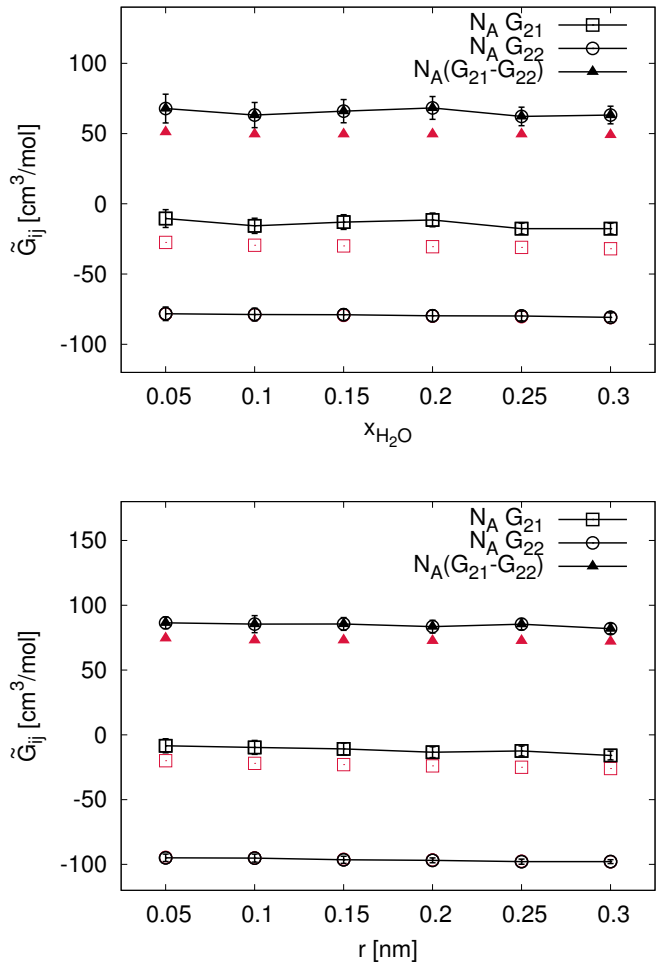

Fig. 5 Top: Rescaled Kirkwood-Buff integrals $\tilde{G}_{22}$, $\tilde{G}_{21}$ and $\tilde{G}_{21}-\tilde{G}_{22}$ for water molecules and ions in EMIM/BF4. Bottom: Scaled Kirkwood-Buff integrals $\tilde{G}_{22}$, $\tilde{G}_{21}$ and $\tilde{G}_{21}-\tilde{G}_{22}$ for water molecules and ions in BMIM/BF4. All data are given for different mole fractions of water. Symbols with solid lines denote simulation results whereas single red symbols represent the corresponding values[20] obtained by the inverse KB approach.

BMIM/BF4 with $\Delta F^{-}_{\mathrm{PMF}} \approx -1.5\,k_BT$ when compared to EMIM/BF4 with $\Delta F^{-}_{\mathrm{PMF}} \approx -1.34\,k_BT$. In contrast, the cation-water potential of mean force is largely comparable in both ILs with $\Delta F^{+}_{\mathrm{PMF}} \approx -0.47\,k_BT$. Compared with the cations, one can safely conclude that a stronger binding between water molecules and BF4 exists.

However, the stronger binding is of minor importance when compared to the water coordination numbers around the individual ions. In Tables 1 (EMIM/BF4) and 2 (BMIM/BF4), we present the water coordination numbers around the anions and the cations in the first hydration shell according to Eqn. (9) with the corresponding distances d_+ and d_- as defined by the local minimum values for the radial distribution functions given in the captions of the tables. Although a linear increase of the coordination numbers around the anions with increasing water mole fraction is evident, the corresponding values are always below unity. The values for the water coordination numbers around the cations

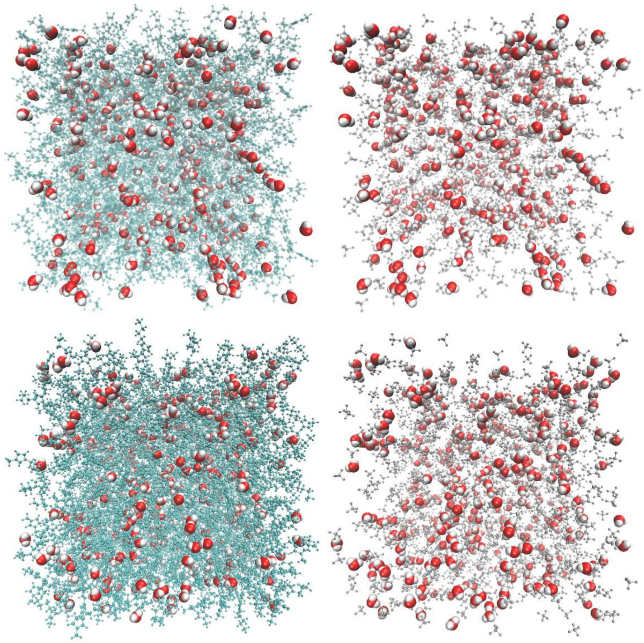

Fig. 6 Top: Snapshots of water molecules (molecular representation) in EMIM/BF4 with EMIM cations (left side) and BF4 anions (right side). Bottom: Snapshots of water molecules in BMIM/BF4 with BMIM cations (left side) and BF4 anions (right side). Both snapshots are given for a water mole fraction $x_{\mathrm{H_2O}} = 0.3$.

also linearly increase from $\langle N_{+1}(d_+)\rangle \approx 0.3$ for the lowest water content to $\langle N_{+1}(d_+)\rangle = 2.0-2.1$ at $\mathrm{x_{H_2O}} = 0.30$ in both ILs. A slightly higher coordination number can be observed for BMIM when compared to EMIM, which can be attributed to the larger molecular size of BMIM and the corresponding larger distances d_+. Although the water binding to the anions is stronger, it

$\mathrm{x_{H_2O}}$	$\langle N_{+1}(d_+)\rangle$	$\langle N_{-1}(d_-)\rangle$
0.05	0.26	0.11
0.10	0.54	0.22
0.15	0.84	0.34
0.20	1.19	0.47
0.25	1.56	0.61
0.30	1.99	0.76

Table 1 Water coordination numbers $\langle N_{j1}(d)\rangle$ for water molecules at different mole fractions in EMIM/BF4 in the first solvent shell around cations ($j=+$) with $d = d_+ = 0.66$ nm and around anions ($j=-$) with $d = d_- = 0.48$ nm according to the results shown in Fig. 7.

can be concluded that most water molecules tend to accumulate around the cations.

In order to study the preferential binding or exclusion of water molecules around the IL ions, we present the values for the corresponding local/bulk partition coefficients (Eqn. (8)) in Fig. 8. As a meaningful criterion for the evaluation of the results, the values for the local/bulk partition coefficient are shown for all regions with $N_{p1}(r)/N_1(r) > 0.005$ for $p=+,-$, which roughly corresponds to $N_{p1}(r) \approx 1$ at the highest water mole fraction $x_{\mathrm{H_2O}} = 0.3$. Taking into account the accumulation of water molecules

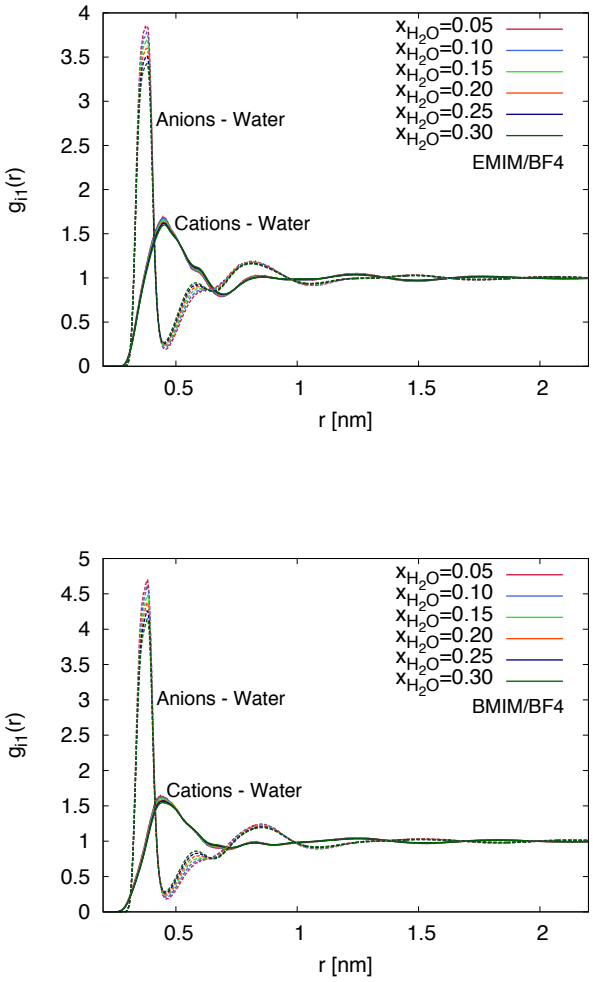

Fig. 7 Top: Radial distribution function (center-of-masses) $g_{+1}(r)$ for EMIM-water pairs (solid lines) and $g_{-1}(r)$ for BF4-water pairs (dashed lines). Bottom: Radial distribution function (center-of-masses) $g_{+1}(r)$ for BMIM-water pairs (solid lines) and $g_{-1}(r)$ for BF4-water pairs (dashed lines). All $g_{+1}(r)$ are given at different water mole fractions.

around the EMIM cations according to the values of $K_{12}^{+}(r) = (\langle N_{+1}(r)\rangle/\langle N_{+2}(r)\rangle/(N_1/N_2)$ (top panel of Fig. 8), it can be clearly seen that important concentration dependent effects are mostly absent. Hence, the values for the local/bulk partition coefficient coincide in both ILs for all values of x_{H_2O}. According to Eqn. (8), it can thus be concluded that higher water concentrations stimulate a linear increase in the amount of water molecules around the cations, which is more favorable than ion accumulation. Values of $K_{12}^{+}(r) \approx 1$ indicate that bulk solution behavior can be found at $r \geq 1.8$ nm, so that the local inhomogeneous region around the cations is defined up to this distance. Furthermore, the presence of a preferential binding mechanism according to $K_{12}^{+}(r) > 1$ can be observed at all distances up to $r \approx 1.0$ nm. The largest deviations from bulk solution behavior can be found at distances $r \leq 1.0$ nm, at which a significant increase of the local/bulk partition coefficient can be observed. These data

x_{H_2O}	$\langle N_{+1}(d_+)\rangle$	$\langle N_{-1}(d_-)\rangle$
0.05	0.27	0.11
0.10	0.56	0.22
0.15	0.88	0.34
0.20	1.24	0.47
0.25	1.64	0.60
0.30	2.09	0.76

Table 2 Water coordination numbers $\langle N_{j1}(d)\rangle$ for water molecules at different mole fractions in BMIM/BF4 in the first solvent shell around cations ($j = +$) with $d = d_+ = 0.72$ nm and around anions ($j = -$) with $d = d_- = 0.48$ nm according to the results shown in Fig. 7.

point to the fact that water molecules, although in small amounts, more preferably accumulate around EMIM and BMIM cations at short distances in comparison with IL ions. Interestingly, the water binding to BMIM cations is more preferable when compared to EMIM cations. These findings explain the lower increase of the cation diffusivities when compared to the diffusional behavior of the anions as shown in Fig. 2.

This effect becomes even more prominent by inspecting $K_{12}^{-}(r) = (\langle N_{-1}(r)\rangle/\langle N_{-2}(r)\rangle/(N_1/N_2)$, shown at the bottom panel of Fig. 8. In agreement with Fig. 7, a pronounced preferential exclusion region of water molecules is observed around the tetrafluoroborate anions at distances $r = 0.65 - 0.85$ for both ILs. The strong increase at shorter distances is represented by a total number of $\langle N_{-1}\rangle \leq 1$ water molecules in this region, which highlights the fact that a preferential binding between anions and water molecules at short distances due to $K_{12}^{-}(r) > 0$ is of minor importance. Furthermore, a minor water accumulation region can be observed at distances $r = 0.8 - 1.2$ nm around the anions. Due to the repulsive behavior of BF4 at intermediate distances, it can be inferred that the accumulation in this region is induced by the crucial interplay between anions and cations. The pronounced long-range order in ILs around solutes[44,64] can also be observed due to varying values for the local/bulk partition coefficient up to distances of $r = 2.2$ nm.

As a means to evaluate the occurrence of water-rich regions in more detail, the corresponding values for G_{11} and G_{12} can be analyzed. Although well-defined in inverse KB theory (section 2 and Refs. 20,21), the calculation of these values is a challenging task in computer simulations. The low statistical validity of these values can be mostly attributed to the limited time and length scale in numerical procedures. As the evaluation of the KB integral between water molecules G_{11} at low mole fraction is too exhaustive, we compute the more-robust values for the local/bulk partition coefficient $K_{12}^{1}(r) = (\langle N_{11}(r)\rangle/\langle N_{12}(r)\rangle/(N_1/N_2)$, in order to provide statistically more reliable results. The corresponding outcomes for EMIM/BF4 are shown in the top panel of Fig. 9. In agreement with the water-cation binding behavior (top panel of Fig. 8), the values for $K_{12}^{1}(r)$ are comparable, which indicates that water-water pairing is a meaningful process at higher water mole fractions. Moreover, it can be seen that the values of K_{12}^{1} are positive at all distances, indicating a preferential binding behavior. Slight concentration dependent effects for water molecules in

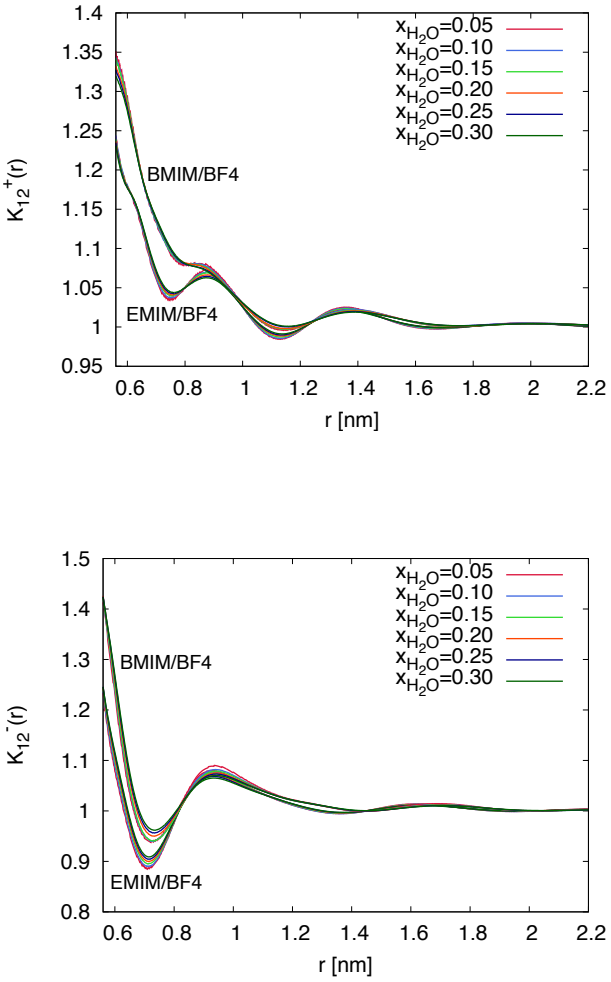

Fig. 8 Top: Local/bulk partition coefficient K_{12}^{+} according to Eqn. (8) for water molecules around EMIM and BMIM cations. Bottom: Local/bulk partition coefficient K_{12}^{-} according to Eqn. (8) for water molecules around BF4 anions in EMIM/BF4 and BMIM/BF4. The data are presented at different water mole fractions.

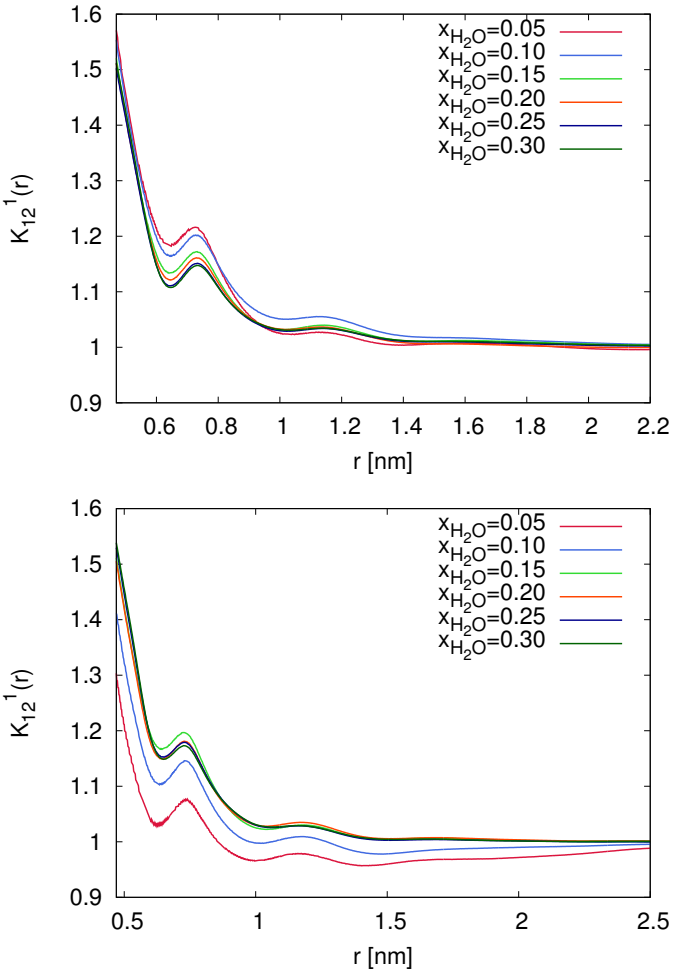

Fig. 9 Top: Local/bulk partition coefficient K_{12}^{1} according to Eqn. (8) for water-water binding in presence of EMIM/BF4. Bottom: Local/bulk partition coefficient for K_{12}^{1} according to Eqn. (8) for water-water binding in presence of BMIM/BF4. The data are presented at different water mole fractions.

EMIM/BF4 can be seen at water-water distances between 0.6 to 1.4 nm, where higher mole fractions reveal a weak lowering of the local/bulk partition coefficient values.

Different results can be observed for BMIM/BF4 (bottom of Fig. 9). It can be seen that significant concentration dependent effects are evident from distances $r = 0.4$ upwards. Hence, for water mole fractions $x_{H_2O} = 0.05$ and $x_{H_2O} = 0.10$, significantly lower values can be observed, which indicates that water pairing when comparted with water-ion pairing is less favorable at these mole fractions. Furthermore, due to the comparable peak values at $r \approx 0.8$ nm with the results shown at the top panel of Fig. 8, one can clearly see that water pairing is aided by the ions. Thus, the anions and the cations attract water molecules according to Fig. 7 and at the corresponding higher mole fractions of water, water pairs start to form around EMIM and BMIM.

In order to study the structural arrangement of clustered water molecules in more detail, we calculated the fraction of water molecules in monomeric, dimeric, trimeric and higher order clusters. For the corresponding analysis, we counted the number of water molecules whose oxygen atoms are located within an intermolecular distance of 0.35 nm. Due to the limited statistical accuracy, trimeric and tetrameric water clusters are combined as one reference group. The results are depicted in Fig. 10. It can be clearly seen that for mole fractions $x_{H_2O} \leq 0.15$, over 75% of water molecules are in the monomeric state. This can be safely attributed to the low concentration of water molecules in the solution. For higher mole fractions, the corresponding probability for the monomeric state linearly decreases from over 90% ($x_{H_2O} = 0.05$) to 48% at $x_{H_2O} \leq 0.30$. Although the corresponding probabilities for BMIM/BF4 are slightly higher (around 2-3% for all mole fractions, whereas the dimeric form is less favorable compared to EMIM/BF4), an identical linear decrease for the monomeric water state can be observed. Interestingly, a non-linear increase can be observed for the occurrence of water dimers and higher order clusters. The results reveal an in-

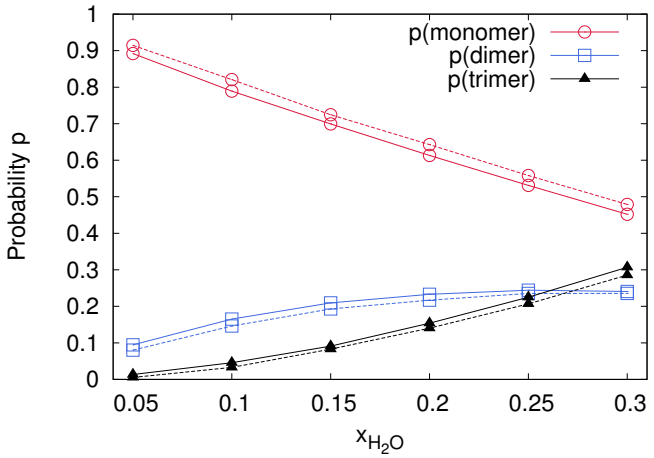

Fig. 10 Probability of water molecules in monomeric p(monomer), dimeric p(dimer) and trimeric/tetrameric p(trimer) arrangement in EMIM/BF4 (solid line) and BMIM/BF4 (dashed line) for different water mole fractions.

crease of the dimer probability from 9% at $x_{H_2O} = 0.05$ to 22% at $x_{H_2O} = 0.20$ from which it saturates to a constant value at higher mole fractions. A strong increase of the trimeric and higher order water cluster state from roughly 0% at $x_{H_2O} = 0.05$ to 30% at $x_{H_2O} = 0.30$ can be also observed. Differences in p(trimer) between EMIM/BF4 and BMIM/BF4 can be mainly observed from $x_{H_2O} \geq 0.20$ upwards with a slightly higher value for EMIM/BF4. The results indicate that differences in the formation of water-rich regions between EMIM/BF4 and BMIM/BF4 are rather marginal. Furthermore, it becomes evident that water molecules tend to form higher order water clusters instead of a dimer state at $x_{H_2O} \geq 0.25$. Based on these results, we can conclude that the formation of water clusters is linearly driven by the higher concentration of water molecules in the solution.

4.5 Partial structure factors

In order to study the global configuration of the systems, we calculated the partial structure factors according to Eqn. (20). Thus, we evaluated the partial structure factors $S_{\pm 1}$ of water molecules around cations and anions as reference. The corresponding results are depicted in the top (S_{+1}) and the bottom (S_{-1}) panels of Fig. 11. The results for the cation-cation partial structure factor S_{++} are given in the supporting material and are in agreement with previous results, as it becomes evident that water molecules have a negligible influence on the ion-ion distribution in the solution.

The main peak position for water molecules around IL cations in both IL solutions according to the values of S_{+1} is located at $q \approx 16$ nm^{-1}, corresponding to distances of $r \approx 0.4$ nm. As discussed before, this coincides with a local accumulation of water molecules around the cations. The slightly lower values of S_{-1} in BMIM/BF4 when compared to EMIM/BF4 can be attributed to the larger molecular size of the cations. Moreover, one can observe slight concentration dependent effects, such that a higher water mole fraction corresponds to larger peak values. A pronounced minimum can be observed at $q \approx 9$ nm^{-1}, corresponding to distances of $r \approx 0.7$ nm. Further peaks at lower q values are absent. Concentration dependent variations can be mainly observed at the maximum peak positions and in the region $q = 7 - 14$ nm^{-1}. The variation of the maximum peak values can be related to the formation of water clusters due to the presence of more water molecules. This assumption also explains the slight decrease of S_{+1} values in the region $q = 7 - 14$ nm^{-1} for higher water concentrations. Nevertheless, it has to be pointed out that the maximum peak values are only slightly higher than unity, whereas all other values are below. Hence, it can be safely argued, based on our previous findings, that the most probable location of water molecules can be found around cations at short distances. Further far-field ordering processes are mainly absent. Accordingly, the formation of water clusters is a local process, which does not affect water pairing at larger distances.

The anion-water partial structure factors S_{-1} show less pronounced peaks. An increase in these can be only observed at $q \approx 7 - 9$ nm^{-1}. This corresponds to $r \approx 0.7 - 1$ nm, which is the characteristic length scale around tetrafluoroborate anions in agreement with Fig. 8. In fact, the maximum peaks occur at slightly lower q values for BMIM/BF4 when compared to EMIM/BF4. This indicates that the local organization of the BMIM cations, which are larger than the EMIM cations, has a pronounced influence on the water distribution around the anions, as discussed previously. The large distance associated with the maximum peaks reveals the absence of a pronounced local water binding to the anions, in agreement with the low coordination numbers shown in Tables 1 and 2. Thus, the partial structure factor analysis also reveals that water mainly binds to the IL cations. Finally, all values for the partial structure factors can be found in the range $S_{\pm 1} = 0.8 - 1.1$. This indicates that the aqueous IL solution can be mostly regarded as ideal although slight water binding effects, resulting in the formation of lower order water clusters can be observed at higher water content.

5 Summary and Conclusion

We performed atomistic MD simulations in order to compare direct and inverse KB approaches for the study of water structural properties in two ionic liquids, 1-ethyl-3-methylimidazolium tetrafluoroborate and 1-butyl-3-methylimidazolium tetrafluoroborate. The outcomes of our simulations reveal that the corresponding KB integrals are in quantitative agreement with those obtained by an inverse KB approach. In more detail, the corresponding values for the individual excess volumes reveal that the water-water KB integrals are negative for all mole fractions in agreement with the ion-ion KB integrals. The large negative values for G_{22} can be mostly attributed to the large size of the like-wise charged cations, which becomes specifically evident for the more negative values of BMIM/BF4. As a consequence from $G_{22} \ll G_{21}$, the corresponding differences between $G_{21} - G_{22}$ are positive. At a first glance, this implies that water molecules preferentially bind to ions. Further, analysis revealed that this effect is mostly governed by the pronounced negative values of the ion-ion KB integrals. As a consequence, the observed finding can be purely related to the large size of the IL ions. A significant influ-

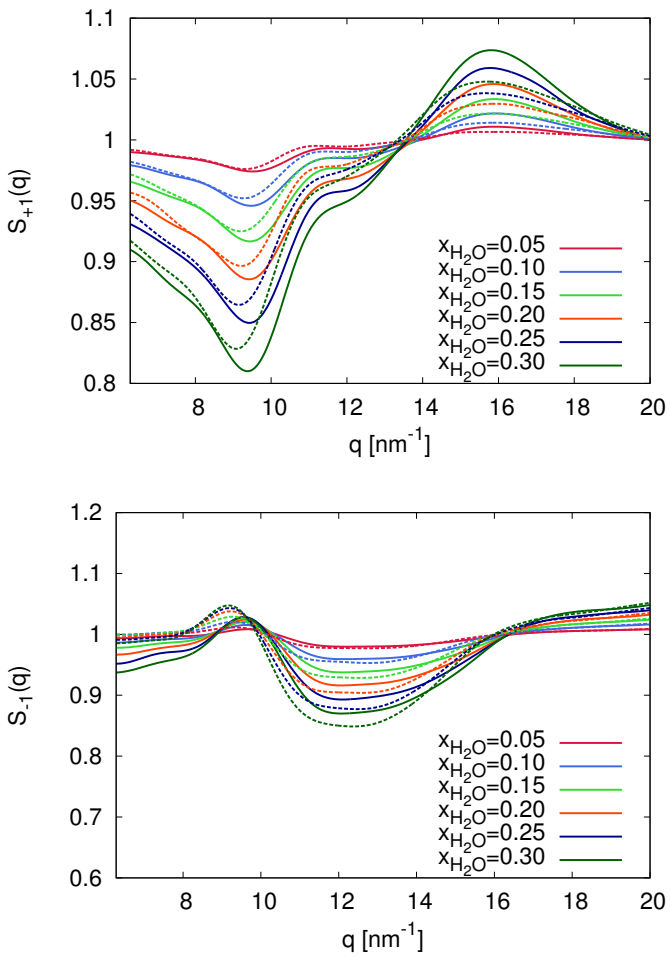

Fig. 11 Top: Partial structure factors S_{+1} for water molecules around IL cations, the latter taken as the reference molecules. Bottom: Partial structure factors S_{-1} for water molecules around BF4, the latter taken as the reference molecules. The data in both panels are shown for different water mole fractions. The solid lines represent the results for EMIM/BF4 whereas dashed lines correspond to the BMIM/BF4 mixtures.

ence on the KB integrals with increasing mole fractions of water was not observed.

Inspection of the dynamic properties showed that the presence of higher water mole fractions mostly influences the diffusivity of the IL species. Our findings are in good agreement with previous studies showing that the increase of the diffusion coefficients can be mainly attributed to the lower viscosity of the solution [38,120].

In order to understand the properties of the aqueous IL solution in more detail, we studied the local accumulation of water molecules around the ion species. The results for the local/bulk partition coefficients and the water coordination numbers highlight a preferential accumulation of water around the IL cations. Moreover, a slightly higher number of water molecules around BMIM cations at short distances when compared to EMIM was observed. Although the values for the water coordination numbers are higher for the cations, a stronger binding potential of mean force was observed for the anions. As a consequence, if water molecules are attracted to anions, which is less likely compared to cations, they are stronger bound and thus rationalize the pronounced hygroscopicity of the studied ILs. In fact, it also can be speculated that water removal for technological applications by temperature increase is also hindered by anion-water pairs. In addition, the water structure analysis pointed out that nearly half of all water molecules, even at the highest mole fraction of $x_{H_2O} = 0.3$, do not form dimeric or higher order structures. With increasing concentration of water, the corresponding monomeric occurrence probability linearly decreases while water dimer and water trimer cluster contributions increase non-linearly. Accordingly, a complex interplay between water-cation and water-anion effects dominate the resulting behavior. Our data thus explain the high hygroscopicity of hydrophobic ILs, which is mainly driven by a strong binding to the anions and the pronounced accumulation around the cations.

Although our simulation data are in good agreement with experimental results, it has to be mentioned that some properties of water/IL mixtures are not well reproduced by classical atomistic force fields. Previous *ab initio* molecular dynamics simulations of water molecules in 1-methyl-3-ethylmethylimidazolium acetate [122] highlighted the pronounced influence of hydrogen bonds and depolarization effects. Hence, it was observed that strong hydrogen bonds exist between the IL anions and cations, which questions the general aprotic behavior of the IL. Furthermore, it was reported that IL cations can exhibit a depolarization effect on water molecules. Thus, the dipole moment of water decreases with increasing IL concentration in several aprotic and protic ILs [122–124], which can be counteracted in presence of strong hydrogen bond acceptor anions. Another interesting effect is also the formation of carbenes in presence of water [122]. It is clear that all these complex mechanisms cannot be captured by non-reactive classical molecular dynamics simulations. However, based on our approach, it can be nevertheless concluded that basic properties of water distribution in ILs are in good agreement with experimental findings.

In summary, direct and inverse KB approaches with subsequent analysis of molecular dynamics simulations can be used to obtain reliable insights into the properties of solutions. For the understanding of aqueous IL solutions, it is necessary to match molecular dynamics simulations to experimental results, for instance inverse KB integrals. Vice versa, molecular simulations provide insights into the properties of solutions which are on the other hand inaccessible to inverse KB approaches. With a combination of both approaches, more light can be shed on the properties of these fascinating and complex solutions, in view of the application of ILs in electrochemical storage systems or in synthesis procedures.

6 Acknowledgments

We thank Volker Lesch, Frank Uhlig, Johannes Zeman, Anand Narayanan Krishnamoorthy, Julian Michalowsky, Luis M. Varela, Christian Schröder, José Nuno Canongia Lopes and Christian Holm for valuable hints and discussions. Financial funding is gratefully acknowledged from the Deutsche Forschungsgemeinschaft through the SFB 716 and the cluster of excellence SimTech (EXC 310).

References

1 J. D. Holbrey, W. M. Reichert, S. K. Spear, R. P. Swatloski, M. B. Turner and A. E. Visser, ACS symposium series, 2003.

2 C. Reichardt and T. Welton, *Solvents and solvent effects in organic chemistry*, John Wiley & Sons, 2011.

3 P. Wasserscheid and T. Welton, *Ionic liquids in synthesis*, John Wiley & Sons, 2008.

4 M. Galiński, A. Lewandowski and I. Stepniak, *Electrochim. Acta*, 2006, **51**, 5567–5580.

5 A. Matic and B. Scrosati, *MRS Bullet.*, 2013, **38**, 533–537.

6 T. Yasuda and M. Watanabe, *MRS Bullet.*, 2013, **38**, 560–566.

7 H. Weingärtner, *Angew. Chem. Int. Ed.*, 2008, **47**, 654–670.

8 K. R. Seddon, A. Stark and M.-J. Torres, *Pure Appl. Chem.*, 2000, **72**, 2275–2287.

9 L. Cammarata, S. Kazarian, P. Salter and T. Welton, *Phys. Chem. Chem. Phys.*, 2001, **3**, 5192–5200.

10 J. L. Anthony, E. J. Maginn and J. F. Brennecke, *J. Phys. Chem. B*, 2001, **105**, 10942–10949.

11 S. Rivera-Rubero and S. Baldelli, *J. Am. Chem. Soc.*, 2004, **126**, 11788–11789.

12 R. Lynden-Bell, J. Kohanoff and M. Del Popolo, *Farad. Discuss.*, 2005, **129**, 57–67.

13 W. Jiang, Y. Wang and G. A. Voth, *J. Phys. Chem. B*, 2007, **4**, 6.

14 B. Bhargava, Y. Yasaka and M. L. Klein, *Chem. Commun.*, 2011, **47**, 6228–6241.

15 T. Méndez-Morales, J. Carrete, O. Cabeza, L. J. Gallego and L. M. Varela, *J. Phys. Chem. B*, 2011, **115**, 6995–7008.

16 Y. Kohno and H. Ohno, *Chem. Commun.*, 2012, **48**, 7119–7130.

17 R. Hayes, S. Imberti, G. G. Warr and R. Atkin, *Angew. Chem. Int. Ed.*, 2012, **51**, 7468–7471.

18 K. A. Maerzke, G. S. Goff, W. H. Runde, W. F. Schneider and E. J. Maginn, *J. Phys. Chem. B*, 2013, **117**, 10852–10868.

19 G. Feng, X. Jiang, R. Qiao and A. A. Kornyshev, *ACS Nano*, 2014, **8**, 11685–11694.

20 J. E. Reid, A. J. Walker and S. Shimizu, *Phys. Chem. Chem. Phys.*, 2015, **17**, 14710–14718.

21 J. E. S. J. Reid, R. J. Gammons, J. M. Slattery, A. J. Walker and S. Shimizu, *J. Phys. Chem. B*, 2017, **121**, 599–609.

22 H. Katayanagi, K. Nishikawa, H. Shimozaki, K. Miki, P. Westh and Y. Koga, *J. Phys. Chem. B*, 2004, **108**, 19451–19457.

23 Y. Wang, H. Li and S. Han, *J. Phys. Chem. B*, 2006, **110**, 24646–24651.

24 T. Singh and A. Kumar, *J. Phys. Chem. B*, 2007, **111**, 7843–7851.

25 Y. Jeon, J. Sung, D. Kim, C. Seo, H. Cheong, Y. Ouchi, R. Ozawa and H.-o. Hamaguchi, *J. Phys. Chem. B*, 2008, **112**, 923–928.

26 M. Moreno, F. Castiglione, A. Mele, C. Pasqui and G. Raos, *J. Phys. Chem. B*, 2008, **112**, 7826–7836.

27 H. Kato, K. Nishikawa, H. Murai, T. Morita and Y. Koga, *J. Phys. Chem. B*, 2008, **112**, 13344–13348.

28 R. Hayes, G. G. Warr and R. Atkin, *Chem. Rev.*, 2015, **115**, 6357–6426.

29 A. R. Porter, S. Y. Liem and P. L. Popelier, *Phys. Chem. Chem. Phys.*, 2008, **10**, 4240–4248.

30 S. Feng and G. A. Voth, *Fluid Phase Equilib.*, 2010, **294**, 148–156.

31 M. Haberler, C. Schröder and O. Steinhauser, *J. Chem. Theo. Comput.*, 2012, **8**, 3911–3928.

32 M. Haberler and O. Steinhauser, *Phys. Chem. Chem. Phys.*, 2011, **13**, 17994–18004.

33 J. G. Huddleston, A. E. Visser, W. M. Reichert, H. D. Willauer, G. A. Broker and R. D. Rogers, *Green Chem.*, 2001, **3**, 156–164.

34 J. N. Canongia Lopes and A. A. Pádua, *J. Phys. Chem. B*, 2006, **110**, 19586–19592.

35 A. Menjoge, J. Dixon, J. F. Brennecke, E. J. Maginn and S. Vasenkov, *J. Phys. Chem. B*, 2009, **113**, 6353–6359.

36 E. Rilo, J. Pico, S. García-Garabal, L. Varela and O. Cabeza, *Fluid Phase Equilib.*, 2009, **285**, 83–89.

37 E. Rilo, J. Vila, S. García-Garabal, L. Varela and O. Cabeza, *J. Phys. Chem. B*, 2013, **117**, 1411–1418.

38 M. S. Kelkar and E. J. Maginn, *J. Phys. Chem. B*, 2007, **111**, 4867–4876.

39 C. E. S. Bernardes, K. Shimizu and J. N. C. Lopes, *J. Phys. Condes. Matter*, 2015, **27**, 194116.

40 K. Saihara, Y. Yoshimura, S. Ohta and A. Shimizu, *Sci. Rep.*, 2015, **5**, 10619.

41 T. A. Fadeeva, P. Husson, J. A. DeVine, M. F. Costa Gomes, S. G. Greenbaum and E. W. Castner Jr, *J. Chem. Phys.*, 2015, **143**, 064503.

42 R. Patel, M. Kumari and A. B. Khan, *Appl. Biochem. Biotechnol.*, 2014, **172**, 3701–3720.

43 H. Zhao, *J. Chem. Technol. Biotechnol.*, 2015, **91**, 25–50.

44 V. Lesch, A. Heuer, C. Holm and J. Smiatek, *Phys. Chem. Chem. Phys.*, 2015, **17**, 8480–8490.

45 H.-J. Tung and J. Pfaendtner, *Mol. Syst. Des. Eng.*, 2016, **1**, 382–390.

46 C. Schröder, *Top. Curr. Chem.*, 2017, **375**, 25.

47 J. Smiatek, *J. Phys. Condens. Matter*, 2017, **29**, 233001.

48 D. Constantinescu, H. Weingärtner and C. Herrmann, *Angew. Chem. Int. Ed.*, 2007, **46**, 8887–8889.

49 Z. Yang, *J. Biotechnol.*, 2009, **144**, 12–22.

50 Z. Yang, X.-J. Liu, C. Chen and P. J. Halling, *Biochim. Biophys. Acta*, 2010, **1804**, 821–828.

51 A. Kumar and P. Venkatesu, *Process Biochem.*, 2014, **49**, 2158–2169.

52 M. Senske, D. C. Aruxandei, M. Havenith, H. Weingärtner, C. Herrmann and S. Ebbinghaus, *Biophys. J.*, 2016, **110**, 212a.

53 M. Senske, D. Constantinescu-Aruxandei, M. Havenith, C. Herrmann, H. Weingärtner and S. Ebbinghaus, *Phys. Chem. Chem. Phys.*, 2016, **18**, 29698–29708.

54 C. Hanke, N. Atamas and R. Lynden-Bell, *Green Chem.*, 2002, **4**, 107–111.

55 J. L. Anthony, J. L. Anderson, E. J. Maginn and J. F. Brennecke, *J. Phys. Chem. B*, 2005, **109**, 6366–6374.

56 L. Crowhurst, P. R. Mawdsley, J. M. Perez-Arlandis, P. A. Salter and T. Welton, *Phys. Chem. Chem. Phys.*, 2003, **5**, 2790–2794.

57 S. M. Urahata and M. C. Ribeiro, *J. Chem. Phys.*, 2004, **120**, 1855–1863.

58 A. A. Pádua, M. F. Costa Gomes and J. N. Canongia Lopes, *Acc. Chem. Res.*, 2007, **40**, 1087–1096.

59 T. G. Youngs, J. D. Holbrey, M. Deetlefs, M. Nieuwenhuyzen, M. F. Costa Gomes and C. Hardacre, *ChemPhysChem*, 2006, **7**, 2279–2281.

60 T. Youngs, C. Hardacre and J. Holbrey, *J. Phys. Chem. B*, 2007, **111**, 13765–13774.

61 C. Hardacre, J. D. Holbrey, M. Nieuwenhuyzen and T. G. Youngs, *Acc. Chem. Res.*, 2007, **40**, 1146–1155.

62 Z. Terranova and S. Corcelli, *J. Phys. Chem. B*, 2013, **117**, 15659–15666.

63 Z. Terranova and S. Corcelli, *J. Phys. Chem. B*, 2014, **118**, 8264–8272.

64 V. Lesch, A. Heuer, B. R. Rad, M. Winter and J. Smiatek, *Phys. Chem. Chem. Phys.*, 2016, **18**, 28403–28408.

65 J. G. Kirkwood and F. P. Buff, *J. Chem. Phys.*, 1951, **19**, 774–777.

66 D. Hall, *Transact. Farad. Soc.*, 1971, **67**, 2516–2524.

67 K. E. Newman, *Chem. Soc. Rev.*, 1994, **23**, 31–40.

68 R. Chitra and P. E. Smith, *J. Phys. Chem. B*, 2001, **105**, 11513–11522.

69 A. Ben-Naim, *Statistical thermodynamics for chemists and biochemists*, Springer Science & Business Media, Berlin, Germany, 2013.

70 P. E. Smith, *J. Phys. Chem. B*, 1999, **103**, 525–534.

71 P. E. Smith, *J. Phys. Chem. B*, 2004, **108**, 18716–18724.

72 S. Shimizu and D. J. Smith, *J. Chem. Phys.*, 2004, **121**, 1148–1154.

73 J. M. Schurr, D. P. Rangel and S. R. Aragon, *Biophys. J.*, 2005, **89**, 2258–2276.

74 J. Rösgen, B. M. Pettitt and D. W. Bolen, *Biochemistry*, 2004, **43**, 14472–14484.

75 J. Rösgen, B. M. Pettitt and D. W. Bolen, *Biophys. J.*, 2005, **89**, 2988–2997.

76 P. E. Smith, *Biophys. J.*, 2006, **91**, 849–856.

77 J. Rösgen, B. M. Pettitt and D. W. Bolen, *Protein Sci.*, 2007, **16**, 733–743.

78 P. E. Smith, E. Matteoli and J. P. O'Connell, *Fluctuation theory of solutions: applications in chemistry, chemical engineering, and biophysics*, CRC Press, 2013.

79 J. Smiatek, *J. Phys. Chem. B*, 2014, **118**, 771–782.

80 B. M. Baynes and B. L. Trout, *J. Phys. Chem. B*, 2003, **107**, 14058–14067.

81 V. Pierce, M. Kang, M. Aburi, S. Weerasinghe and P. E. Smith, *Cell. Biochem. Biophys.*, 2008, **50**, 1–22.

82 P. G. Kusalik and G. Patey, *J. Chem. Phys.*, 1987, **86**, 5110–5116.

83 V. Pierce, M. Kang, M. Aburi, S. Weerasinghe and P. E. Smith, *Cell. Biochem. Biophys.*, 2008, **50**, 1–22.

84 P. G. Kusalik and G. Patey, *J. Chem. Phys.*, 1988, **88**, 7715–7738.

85 P. G. Kusalik and G. Patey, *J. Chem. Phys.*, 1988, **89**, 5843–5851.

86 P. G. Kusalik and G. Patey, *J. Chem. Phys.*, 1988, **89**, 7478–7484.

87 E. Ruckenstein and I. L. Shulgin, *Adv. Coll. Interface Sci.*, 2006, **123**, 97–103.

88 S. Weerasinghe and P. E. Smith, *J. Chem. Phys.*, 2003, **119**, 11342–11349.

89 M. B. Gee, N. R. Cox, Y. Jiao, N. Bentenitis, S. Weerasinghe and P. E. Smith, *J. Chem. Theory Comput.*, 2011, **7**, 1369–1380.

90 M. Fyta and R. R. Netz, *J. Chem. Phys.*, 2012, **136**, 124103.

91 S. K. Schnell, T. J. Vlugt, J.-M. Simon, D. Bedeaux and S. Kjelstrup, *Mol. Phys.*, 2012, **110**, 1069–1079.

92 P. KruÌĹger, S. K. Schnell, D. Bedeaux, S. Kjelstrup, T. J. Vlugt and J.-M. Simon, *J. Phys. Chem. Lett.*, 2012, **4**, 235–238.

93 S. K. Schnell, P. Englebienne, J.-M. Simon, P. Krüger, S. P. Balaji, S. Kjelstrup, D. Bedeaux, A. Bardow and T. J. Vlugt, *Chem. Phys. Lett.*, 2013, **582**, 154–157.

94 P. Ganguly and N. F. van der Vegt, *J. Chem. Theory Comput.*, 2013, **9**, 1347–1355.

95 R. Cortes-Huerto, K. Kremer and R. Potestio, *J. Chem. Phys.*, 2016, **145**, 141103.

96 J. Lebowitz and J. Percus, *Phys. Rev.*, 1961, **122**, 1675.

97 E. Courtenay, M. Capp, C. Anderson and M. Record, *Biochemistry*, 2000, **39**, 4455–4471.

98 S. Shimizu, *Proc. Natl. Acad. Sci. USA*, 2004, **101**, 1195–1199.

99 D. Diddens, V. Lesch, A. Heuer and J. Smiatek, *to be submitted*, 2016.

100 S. Micciulla, J. Michalowsky, M. A. Schroer, C. Holm, R. von Klitzing and J. Smiatek, *Phys. Chem. Chem. Phys.*, 2016, **18**, 5324–5335.

101 M. A. Schroer, J. Michalowsky, B. Fischer, J. Smiatek and G. Grübel, *Phys. Chem. Chem. Phys.*, 2016, **18**, 31459–31470.

102 A. Ben-Naim, *J. Chem. Phys.*, 1977, **67**, 4884–4890.

103 B. Doliwa and A. Heuer, *Phys. Rev. Lett.*, 1998, **80**, 4915.

104 D. Van Der Spoel, E. Lindahl, B. Hess, G. Groenhof, A. E. Mark and H. J. Berendsen, *J. Comput. Chem.*, 2005, **26**, 1701–1718.

105 S. Pronk, S. PÃąll, R. Schulz, P. Larsson, P. Bjelkmar, R. Apostolov, M. R. Shirts, J. C. Smith, P. M. Kasson, D. van der Spoel, B. Hess and E. Lindahl, *Bioinformatics*, 2013, **29**, 845.

106 M. J. Abraham, T. Murtola, R. Schulz, S. Páll, J. C. Smith, B. Hess and E. Lindahl, *SoftwareX*, 2015, **1**, 19–25.

107 S. V. Sambasivarao and O. Acevedo, *J. Chem. Theory Comput.*, 2009, **5**, 1038–1050.

108 J. N. Canongia Lopes, J. Deschamps and A. A. Pádua, *J. Phys. Chem. B*, 2004, **108**, 2038–2047.

109 V. Ivantsev, https://github.com/vladislavivanistsev/RTIL-FF/, last accessed on May 117h, 2017.

110 H. Berendsen, J. Grigera and T. Straatsma, *J. Phys. Chem.*, 1987, **91**, 6269–6271.

111 S. Gabl, C. Schröder and O. Steinhauser, *J. Chem. Phys.*, 2012, **137**, 094501.

112 L. Martínez, R. Andrade, E. G. Birgin and J. M. Martínez, *J. Comput. Chem.*, 2009, **30**, 2157–2164.

113 G. Bussi, D. Donadio and M. Parrinello, *J. Chem. Phys.*, 2007, **126**, 014101.

114 M. Parrinello and A. Rahman, *J. Appl. Phys.*, 1981, **52**, 7182–7190.

115 T. Darden, D. York and L. Pedersen, *J. Chem. Phys.*, 1993, **98**, 10089–10092.

116 U. Essmann, L. Perera, M. L. Berkowitz, T. Darden, H. Lee and L. G. Pedersen, *J. Chem. Phys.*, 1995, **103**, 8577–8593.

117 B. Hess, H. Bekker, H. J. C. Berendsen and J. G. E. M. Fraaije, *J. Comput. Chem.*, 1997, **18**, 1463–1472.

118 F. Dommert, K. Wendler, R. Berger, L. Delle Site and C. Holm, *ChemPhysChem*, 2012, **13**, 1625–1637.

119 M. Salanne, *Phys. Chem. Chem. Phys.*, 2015, **17**, 14270–14279.

120 E. Rilo, J. Vila, J. Pico, S. Garcia-Garabal, L. Segade, L. M. Varela and O. Cabeza, *J. Chem. Eng. Data*, 2009, **55**, 639–644.

121 V. Lesch, A. Heuer, V. A. Tatsis, C. Holm and J. Smiatek, *Phys. Chem. Chem. Phys.*, 2015, **17**, 26049–26053.

122 M. Brehm, H. Weber, A. S. Pensado, A. Stark and B. Kirchner, *Phys. Chem. Chem. Phys.*, 2012, **14**, 5030–5044.

123 C. Spickermann, J. Thar, S. Lehmann, S. Zahn, J. Hunger, R. Buchner, P. Hunt, T. Welton and B. Kirchner, *J. Chem. Phys.*, 2008, **129**, 104505.

124 S. Zahn, K. Wendler, L. Delle Site and B. Kirchner, *Phys. Chem. Chem. Phys.*, 2011, **13**, 15083–15093.